Applied Catalysis B: Environmental 194 (2016) 105–110

Contents lists available at ScienceDirect

Applied Catalysis B: Environmental

journal homepage: www.elsevier.com/locate/apcatb

# Separation free $C_3N_4/SiO_2$ hybrid hydrogels as high active photocatalysts for TOC removal

Mo Zhang [a,b], Wenjiao Luo [a], Zhen Wei [a], Wenjun Jiang [a], Di Liu [a], Yongfa Zhu [a,*]

[a] Department of Chemistry, Tsinghua University, Beijing, 100084, China
[b] Department of Biophysics and Structural Biology, Institute of Basic Medical Sciences, Chinese Academy of Medical Sciences & School of Basic Medicine, Peking Union Medical College, Beijing, 100730, China

ARTICLE INFO

*Article history:*
Received 8 March 2016
Received in revised form 22 April 2016
Accepted 25 April 2016
Available online 27 April 2016

*Keywords:*
$C_3N_4/SiO_2$
Hybrid hydrogel
Photocatalysis
TOC removal
Separation free

ABSTRACT

The separation free graphitic carbon nitride/$SiO_2$ ($C_3N_4/SiO_2$) hybrid hydrogels with three-dimensional (3D) network structures have been prepared via alkali-solution and acid-gel process. The hybrid hydrogels perform enhanced ability to absorb and in-situ degrade refractory organic pollutants, such as coking wastewater and phenol. Due to the 3D network structures of $C_3N_4/SiO_2$ hybrid hydrogels, they show efficient pollutants removal ability by synergistic effect of adsorption and in-situ photocatalytic degradation. The total organic carbon content (TOC) of coking wastewater is reduced by 33% with $C_3N_4/SiO_2$ hybrid hydrogel, which is 5 times of pure g-$C_3N_4$. The removal abilities of phenol and methylene blue (MB) via hybrid hydrogels are 3.1 and 6 times of pure g-$C_3N_4$ respectively. The 3D network structures guarantee $C_3N_4/SiO_2$ hybrid hydrogels to be continuously used without adsorption saturation and separation from water, avoiding the photocatalysts aggregation and secondary pollution.



## 1. Introduction

Recently, the problems of environmental pollution have attracted extensive attention due to their threat to human health and sustainable development [1–4]. With the development of industry, refractory organic pollutants are produced inevitably. The effective treatment of water pollution has become one of the most concerned research topics [5–7]. Photocatalysts can degrade the pollutants under light irradiation, which is an ideal energy saving and environmental protecting method for water purification [8–11]. Among all the photocatalysts, g-$C_3N_4$ has attracted increasing interests as an organic semiconductor photocatalyst with exciting visible light activity and excellent thermal and chemical stability [12–15]. However, the adsorption ability and photocatalytic reaction rate of g-$C_3N_4$ for some pollutants is poor, limiting its photocatalytic activity [16,17]. Previous studies have revealed that adsorption ability of photocatalysts play a key role in their photocatalytic performance [18,19]. Improving the adsorption ability of g-$C_3N_4$ may be an effective measure to enhance its photocatalytic activity. In addition, the imperfect separation of g-$C_3N_4$ nanoparticle from water may lead to secondary pollution. Therefore, a separation free g-$C_3N_4$ material with high adsorption ability is urgent and important.

The 3D hydrogels are one of the most widely used materials for water purification due to their low cost and outstanding performance for water pollutants adsorption and concentration [20–23]. The 3D network structure of hydrogels can not only provide convenient mass transfer channels, but also prevent the materials from dispersing or aggregation in water, greatly simplified the separation of the materials from water [24–27]. However, the pollution problem cannot be solved completely by hydrogels for the organic pollutants just can be concentrated and separated from water rather than degraded to non-polluting molecules. Besides, the adsorption materials cannot be used continuously when they get adsorption saturation. Only undergo tedious desorption process can the adsorption materials be recycled. Therefore, a separation free 3D hydrogel with photocatalytic activity to degrade the pollutants continuously is urgent.

Photocatalysts based hybrid hydrogel materials with both of pollutants adsorption and degradation ability are undoubtedly the most advantageous [28,29]. The organic contaminants can be adsorbed and enriched onto the surface of the photocatalysts through 3D network nanostructure of hybrid hydrogel and then in situ degraded under light irradiation. However, hybrid hydrogels with visible light activity and thermal stability are still challenges. As an environmental friendly material, silicon dioxide ($SiO_2$) hydrogel is widely applied in the fields of biomimetic and biomedical

* Corresponding author.
*E-mail address:* Zhuyf@mail.tsinghua.edu.cn (Y. Zhu).

http://dx.doi.org/10.1016/j.apcatb.2016.04.049
0926-3373/

materials [30–33]. In this paper, a series of novel $C_3N_4/SiO_2$ hybrid hydrogels are prepared and their pollutants removal abilities are determined with coking wastewater, phenol and MB. The hybrid hydrogels show efficient pollutants and TOC removal ability by synergistic effect of adsorption and photocatalytic degradation. Due to their photocatalytic activity and bulk structure, the $C_3N_4/SiO_2$ hybrid hydrogels can be continuously used without adsorption saturation and separation from water.

## 2. Experimental

### 2.1. Preparation of the $C_3N_4/SiO_2$ hybrid hydrogels

$SiO_2$ and dicyandiamide were purchased from Sinopharm Chemical Reagent Corp, P. R. China. All other reagents used in this research were analytically pure and used without further purification.

The g-$C_3N_4$ was prepared by pyrolysis of dicyandiamide in air atmosphere. The typical preparation of g-$C_3N_4$ photocatalysts was as follows: 5 g dicyandiamide was put in a Muffle Furnace and heated from 30 °C to 550 °C with heating rate of 1 °C/min. Then the product was calcined at 550 °C for 4 h to complete the reaction. The yield of the g-$C_3N_4$ was about 25%.

$SiO_2$ and g-$C_3N_4$ nano-particle hydrosol is transformed into hybrid hydrogel with 3D network structure by alkali-solution and acid-gel process. The typical preparation process was as follows: A certain proportion of $SiO_2$ and g-$C_3N_4$ were put in to 3 mL 5 mol $L^{-1}$ NaOH solution and dispersed by ultrasound for 30 min. 3 mol $L^{-1}$ HCl was added drop by drop with stir and the pH of the mixture was adjusted to 4–7 to form $C_3N_4/SiO_2$ hybrid hydrogel. The 50%-$SiO_2/TiO_2$ was prepared by the similar method. 250 mg $TiO_2$ and 250 mg $SiO_2$ were put into 3 mL 5 mol $L^{-1}$ NaOH solution and ultrasound for 30 min. 3 mol $L^{-1}$ HCl was added drop by drop with stir and the pH of the mixture was adjusted to 4–7 to form 50%-$SiO_2/TiO_2$ hybrid hydrogel. For the characterizations, analysis of absorption capability and synergistic effect of adsorption and photocatalytic degradation in static systems of the hybrid hydrogels, $C_3N_4/SiO_2$ hybrid hydrogels were cryodesiccated to form power. For the analysis of the synergistic effect of adsorption and photocatalytic degradation of the hybrid hydrogels in dynamic systems, the 90%-$C_3N_4/SiO_2$ hybrid hydrogel was added in the reactor without further processed.

### 2.2. Characterization

The morphologies of the $SiO_2$-$C_3N_4$ hybrid hydrogels were characterized by a Hitachi SU-8010 Field Emission Gun Scanning Electron Microscopy and a Hitachi HT 7700 electron microscope operated at an accelerating voltage of 100 kV. UV–vis diffuse reflectance spectroscopy was performed on Hitachi U-3010 UV–vis spectrophotometer with $BaSO_4$ as the reference sample. The crystallinity of the hybrid hydrogels were characterized by X-ray diffraction by Bruker D8-advancediffractometer with Cu-Kα radiation (λ = 1.5418 Å). Raman spectra were obtained by microscopic confocal Raman spectrometer (HORIBA HR800) with an excitation of 785 nm laser light. Fourier transform infrared spectra were carried out by Bruker V70 spectrometer and covered the frequency of 4000–600 $cm^{-1}$ with a resolution of 1 $cm^{-1}$. The photocurrents were operated on an electrochemical system (CHI660B, China).

### 2.3. Photocatalytic experiments

The synergistic effect of adsorption and photocatalytic degradation of the hybrid hydrogels in static systems were evaluated by the decomposition of MB and phenol solution in multi-tube agitated reactor (XPA-7). Visible light source was obtained by a 500 W Xe lamp (Institute for Electric Light Sources, Beijing) with a 420 nm cutoff filter, and the average visible light intensity was 35 mW $cm^{-2}$. 25 mg photocatalyst was added into MB solution (50 mL $3 \times 10^{-5}$ mol $L^{-1}$) or 5 ppm phenol solution. The suspensions were magnetically stirred with visible light irradiation. At given time intervals, 3 mL aliquots were sampled and centrifuged to remove the photocatalysts. The MB supernatant liquid was analysed by recording variations of the maximum absorption peak (664 nm for MB) using a Hitachi U-3010 UV–vis spectrophotometer. The chromatographic experiments with HPLC-UV/vis system were carried out with an ultraviolet absorbance detector (K 2501) operated at 275 nm coupled to a Venusil XBP-$C_{18}$ (Agela Technologies Inc.) column. Before the analysis, the samples were filtered through Millipore discs of 0.45 μm to protect the chromatographic column. The mobile phase used for eluting phenol and its degradation intermediates from the HPLC columns consisted of methanol and water (60:40, v/v) at a flow rate of 1 mL/min.

The synergistic effect of adsorption and photocatalytic degradation of the hybrid hydrogels in dynamic systems were evaluated by the decomposition of coking wastewater and $1 \times 10^{-5}$ mol $L^{-1}$ MB solution in a home-made rectangular reactor. 200 mg photocatalyst was added in the reactor. The fresh liquid flows through the reactor with a flow velocity of 0.5 mL/min. The size of the reactor is 4 cm long, 2 cm wide and 1 cm high. The volume of the liquid in the reactor is 8 mL. At certain intervals, 5 mL degraded coking wastewater or 2 mL degraded MB was sampled from the reactor. The aliquots did not need to be centrifuged and were directly analysed. The total organic carbon analyzer (Multi N/C 2100, Analytik Jena AG) was applied to analyse the mineralization degree of coking wastewater. The Hitachi U-3010 UV–vis spectrophotometer was applied to analyse the concentration of MB.

## 3. Results and discussion

The as prepared $C_3N_4/SiO_2$ hybrid hydrogels show enhanced performance in TOC removal of coking wastewater. To investigate the synergy of coking wastewater adsorption and photocatalytic degradation by hybrid hydrogel, a long-time detection in dynamic system is designed. As shown in Fig. 1a, the fresh coking wastewater flows through the rectangular reactor continuously and is collected at certain intervals to test their TOC. Fig. 1b shows that the TOC of the purified water is decreased via adsorption and photocatalytic degradation by hybrid hydrogel and pure g-$C_3N_4$. In the first 25 min, the TOC of the purified water through 90%-$C_3N_4/SiO_2$ is below 4 mg $L^{-1}$, which is much lower than that of pure g-$C_3N_4$ (13 mg $L^{-1}$). With continuous fresh coking wastewater flow in, the TOC of the purified water is increased to a stable value. The pollutants can be absorbed on the hydrogels faster than pure g-$C_3N_4$, and in-situ degraded to form purified water. Due to the excellent synergistic effect of adsorption and photocatalytic degradation of 90%-$C_3N_4/SiO_2$, TOC of coking wastewater can be removed continuously with removal efficient of 33%, which is 5 times of pure g-$C_3N_4$. More interestingly, the bulk structure of hydrogel can prevent it from dispersing in water, avoiding the photocatalysts aggregation and secondary pollution. The $C_3N_4/SiO_2$ hybrid hydrogels exhibit enhanced performance in adsorption and in situ degradation of coking wastewater continuously for a long time.

The $C_3N_4/SiO_2$ hybrid hydrogels exhibit enhanced performance in pollutants removal, such as phenol and MB. $SiO_2$ cannot remove the phenol after the adsorption equilibrium reached in 5 h (Fig. S1). The hybrid hydrogels with low g-$C_3N_4$ content (20%–40%) perform less adsorption capacity and photocatalytic degradation ability, leading to their less pollutants removal ability. As shown in Fig. 2, the 60%–90% $C_3N_4/SiO_2$ hybrid hydrogels shows enhanced performance in phenol removal via synergistic effect of adsorption and

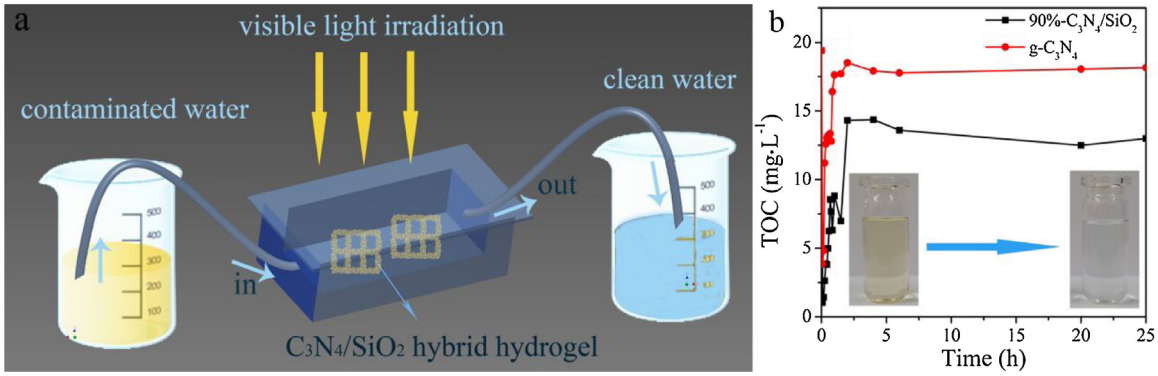


**Fig. 1.** The schematic diagram of the synergistic effect of adsorption and photocatalytic degradation of the hybrid hydrogels in dynamic systems (a) and the TOC of the purified water absorbed and degraded by 90%-$C_3N_4/SiO_2$ and pure g-$C_3N_4$ (b).

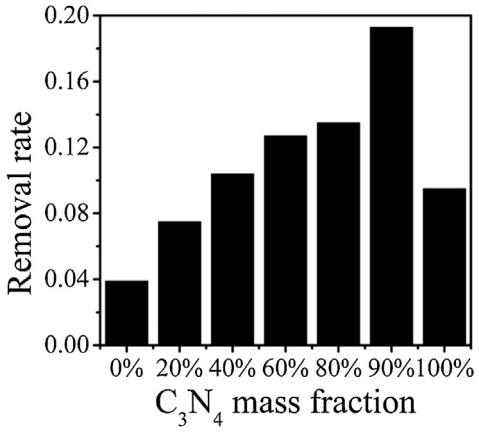


**Fig. 2.** The phenol removal rate by $SiO_2$ hydrogel, hybrid hydrogel and pure g-$C_3N_4$ via synergistic effect of adsorption and photocatalytic degradation in static systems.

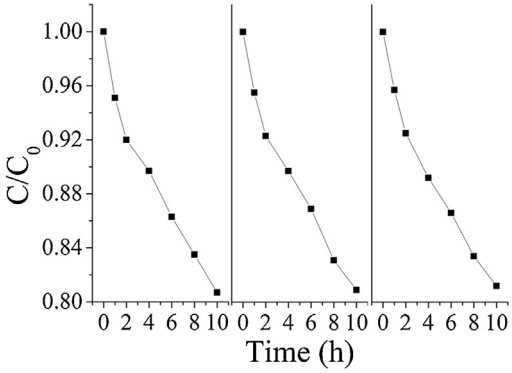


**Fig. 3.** The cycling stability of 90%-$C_3N_4/SiO_2$ hybrid hydrogel for phenol removal.

in-situ photocatalytic degradation, which is 2.1 times as that of pure g-$C_3N_4$. More importantly, the hybrid hydrogels exhibits excellent cycling stability for phenol removal without tedious desorption and recovery process, which is attributed to its photocatalytic degradation ability and 3D bulk structure (Fig. 3).

The variation trend of MB removal by hybrid hydrogels is different from that of phenol. The MB removal ability is decreased with increasing g-$C_3N_4$ content in 5 h (Fig. S2), due to the much better MB adsorption capacity of $SiO_2$ than g-$C_3N_4$. It is observed that the degradation ability of 20% and 40%-$C_3N_4/SiO_2$ hybrid hydrogels is not obvious after adsorption saturation, while 60%–90% $C_3N_4/SiO_2$ hybrid hydrogels perform enhanced degradation ability.

To investigate the synergy of MB adsorption and photocatalytic degradation by hybrid hydrogel, the test method in Fig. 1a in dynamic system is applied. As shown in Fig. 4 the concentration of MB effluent liquid decreases quickly with continuous fresh MB solution through the pure $SiO_2$ and hybrid hydrogel in 4 h, due to their excellent adsorption capacity of MB compared with g-$C_3N_4$. However, concentration of MB effluent liquid through pure agar hydrogel reaches the initial value in the later 6 h because the adsorption equilibrium is reached. With synergy of adsorption and photocatalytic degradation, MB can be removed by 90%-$C_3N_4/SiO_2$ hybrid hydrogel continuously. The removal efficiency of MB by hybrid hydrogel is 6 times as that of pure g-$C_3N_4$. Therefore, with the advantage of enhanced adsorption ability via introduction of $SiO_2$ hydrogel, the $C_3N_4/SiO_2$ hybrid hydrogels exhibit enhanced performance in adsorption and in situ degradation of organic pollutants and improved cycling stability as well.

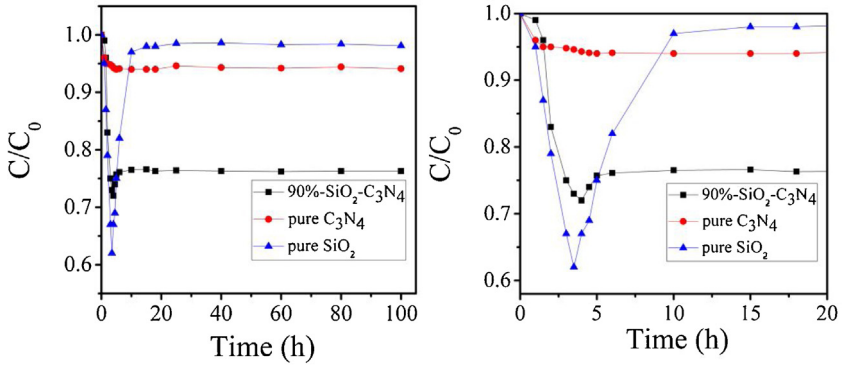


**Fig. 4.** The MB removal abilities of $SiO_2$ hydrogel, hybrid hydrogels and pure g-$C_3N_4$ via synergistic effect of adsorption and photocatalytic degradation in dynamic system.

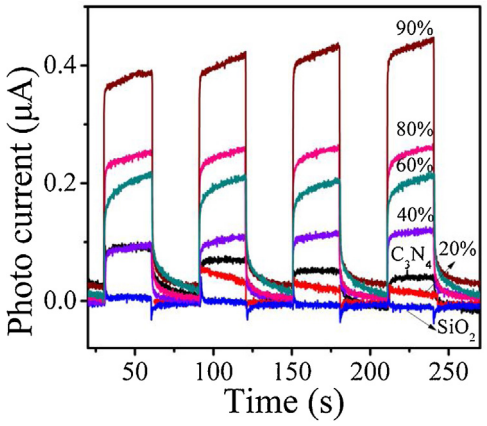


**Fig. 5.** The photocurrent of $SiO_2$ hydrogel, hybrid hydrogels and pure g-$C_3N_4$.

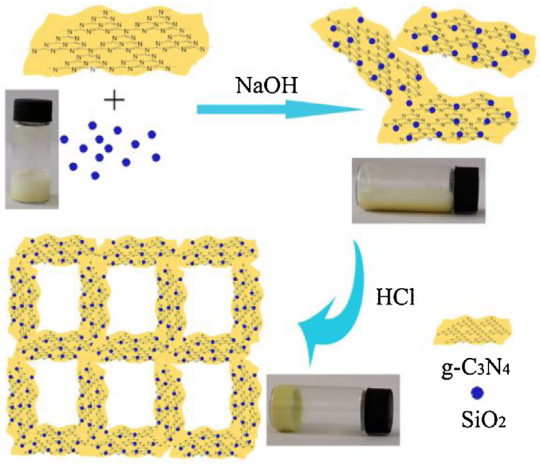


**Fig. 6.** The schematic illustration of preparation of $C_3N_4/SiO_2$ hybrid hydrogel.

The synergy of adsorption and photocatalytic degradation by hybrid hydrogels is further explored by photocurrent. As shown in Fig. 5, little photoelectric response of $SiO_2$ can be observed. The photocurrent of 40%-$C_3N_4/SiO_2$ is similar to that of pure g-$C_3N_4$, while 60%–90% materials perform enhanced photoelectric response, which is consistent with the phenol removal results. The enhanced photocurrent of hybrid hydrogels may due to the improved transition of photogenerated carriers via the porous network structure.

The enhanced performance of hybrid hydrogels in adsorption and in situ degradation of organic pollutants and photogenerated carriers' mobility can be attributed to their 3D network structure. The 3D $C_3N_4/SiO_2$ hybrid hydrogel are prepared via alkali-solution and acid-gel process. As shown in Fig. 6, the hybrid hydrogel can be separated from water by simple taken out instead of complex procedure. The $SiO_2$ sol can transform to gel rapidly by change of pH instead of temperature, indicating the better thermal stability of $SiO_2$ hydrogel compared with agar [29]. Besides, both of the 90%-$C_3N_4/SiO_2$ hybrid hydrogel and 60%-$TiO_2/SiO_2$ hybrid hydrogel show negligible weight loss under the UV irradiation for 1000 h, indicating the light stability of $SiO_2$ mixed with photocatalyst with mild or high mineralization ability (Fig. S3). The enhanced thermal and light stability of $C_3N_4/SiO_2$ hybrid hydrogels suggest their more promising application than agar hybrid hydrogels.

The $SiO_2$ hydrogel Exhibits 3D network structure with cross-linked $SiO_2$ nanospheres (20–50 nm, Fig. S4). With the introduction of g-$C_3N_4$, the mixture is well dispersed after ultrasound, leading to the uniform $C_3N_4/SiO_2$ hybrid hydrogel via alkali-solution and acid-gel process. Fig. 7 shows that g-$C_3N_4$ is coated by $SiO_2$ uniformly and forms network structure by mutual crosslinking $SiO_2$ nanospheres. The network structure of the hybrid hydrogel is less obvious with increasing g-$C_3N_4$ content. When the g-$C_3N_4$ content goes beyond 90%, the 3D network structure will be destroyed to form the bulk morphology as pure g-$C_3N_4$. The structures of hybrid hydrogels can be further confirmed by their TEM images ( Fig. S5). The $SiO_2$ nanospheres are linked with each other and coating g-$C_3N_4$, as the link bridge of g-$C_3N_4$ particles.

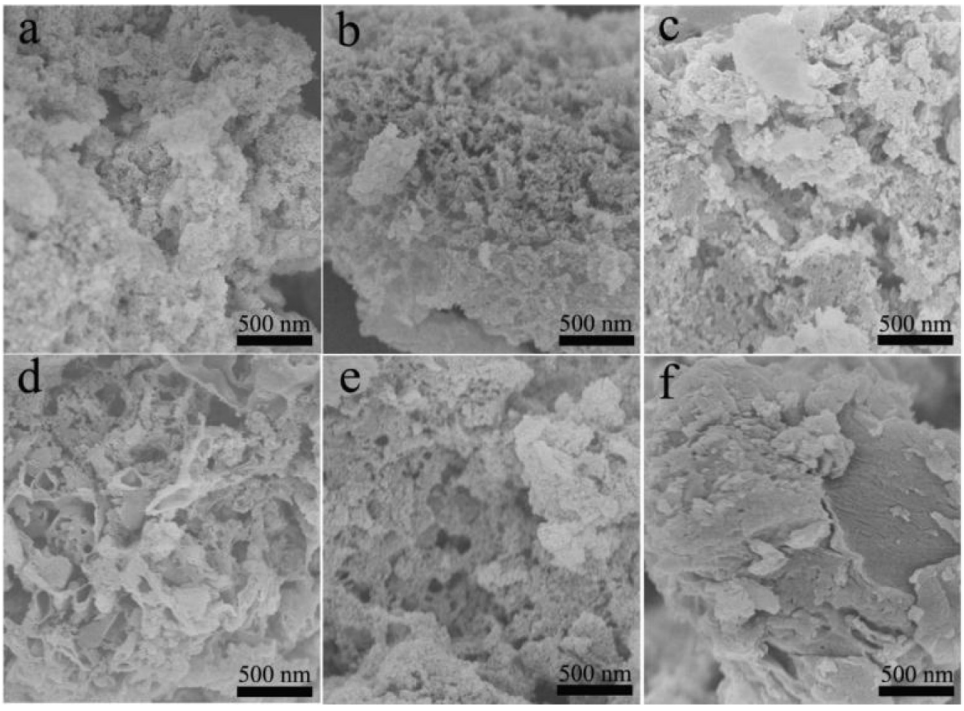


**Fig. 7.** The SEM images of $C_3N_4/SiO_2$ hybrid hydrogels (20%, 40%, 60%, 80% and 90%, a–e) and pure g-$C_3N_4$ (f).

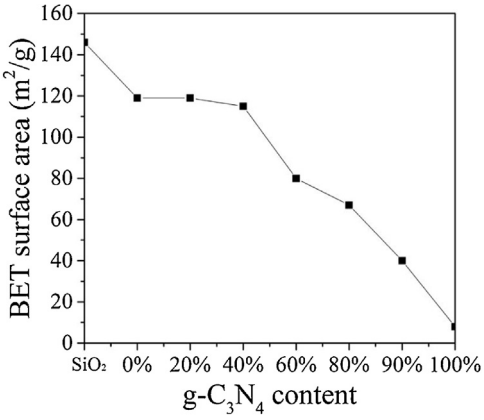


**Fig. 8.** BET specific surface area of $C_3N_4/SiO_2$ hybrid hydrogels and pure g-$C_3N_4$.

Brunauer-Emmett-Teller (BET) measurements revealed the progressively increasing surface areas of $C_3N_4/SiO_2$ prepared with increased mass fraction of $SiO_2$. As shown in Fig. 8, the surface area of $SiO_2$ nano-particle is 146 $m^2\,g^{-1}$, and the surface area of $SiO_2$ hydrogel is about 120 $m^2\,g^{-1}$, indicating the decrease of the surface area of $SiO_2$ nano-particle by crosslinking. With increasing g-$C_3N_4$ content, the specific surface areas of hybrid hydrogels are decreased gradually. Even so, the surface area of 90%-$C_3N_4/SiO_2$ is about 8 times of pure g-$C_3N_4$. The obvious increase of surface area by introduction of $SiO_2$ hydrogel may be attributed to the large surface area of $SiO_2$ and 3D network structure of hybrid hydrogels. The 3D network structure and obvious increase surface area of hybrid hydrogels provide guarantee for their enhanced adsorption and in situ degradation of organic pollutants.

As shown in the X-ray diffraction (XRD) patterns (Fig. S6), $SiO_2$ is amorphous without obvious XRD peak. With increasing g-$C_3N_4$ content, two peaks at 13.1° (100) and 27.5° (002) of the hybrid hydrogels are gradually obvious, corresponding to the in-plane ordering of tri-s-triazine units and graphitic structure of g-$C_3N_4$ [34,35]. The peak intensities are enhanced with the increasing g-$C_3N_4$ content, indicating the higher structure order of hybrid hydrogels with increasing content of g-$C_3N_4$.

The structure of hybrid hydrogels can be further confirmed by FTIR and Raman spectra. The bands in FTIR spectra at 1200–1600 $cm^{-1}$ and 806 $cm^{-1}$ for g-$C_3N_4$ can be attributed to the stretching of aromatic CN heterocycle and the breathing of the triazine unit [36] (Fig. S7). The bands are sharper with increased g-$C_3N_4$ content. Thus, the bands of $SiO_2$ at 1050 $cm^{-1}$ originated from Si-O-Si [37] are getting subtle with large amounts of g-$C_3N_4$. In addition, the characteristic Raman spectra of hybrid hydrogels are similar to that of pure g-$C_3N_4$ [38] (Fig. S8). The shaper bands are attributed to more ordered packing of g-$C_3N_4$ with increasing g-$C_3N_4$ content, which is consistent with the results of XRD and FTIR.

The zeta potentials of hybrid hydrogels measured in aqueous solutions at pH 6.5 (Fig. S9). The zeta potential of $SiO_2$ is about 0. The obvious increase can be observed with increasing g-$C_3N_4$ content, indicating more stability of the materials in the condition. The adsorption capacity of $SiO_2$ aerogel, 90%-$C_3N_4/SiO_2$ hybrid aerogel and pure g-$C_3N_4$ are compared by equilibrium adsorption isotherm studies (Figs. S10 and S11). The adsorption capacities of 90%-$C_3N_4/SiO_2$ hybrid aerogel are about 3.5 and 48 mg $g^{-1}$ for phenol and MB, which are 9 and 1.8 times as that of pure g-$C_3N_4$. The $SiO_2$ aerogel performs the best adsorption capacity, indicating the adsorption capacities of materials are not related to their zeta potentials.

## 4. Conclusion

The series $C_3N_4/SiO_2$ hybrid hydrogels are prepared by alkali-solution and acid-gel process. The $C_3N_4/SiO_2$ hybrid hydrogels show enhanced performance in photocatalytic degradation of coking wastewater, phenol and MB under visible light via synergistic effect of adsorption and photocatalysis. The hybrid hydrogel exhibits excellent cyclic stability and can be used continuously without adsorption saturation. The novel g-$C_3N_4$ based 3D hybrid hydrogels is facile to be separated from water to avoid secondary pollution, which are promising materials used in the treatment of water pollutants.

## Supporting information

Additional figures for the phenol and MB adsorption ability of the $C_3N_4/SiO_2$ hybrid hydrogels, TEM images, XRD patterns, FTIR, Raman and UV–vis reflectance spectra associated with this article can be found in the online version.

## Acknowledgments

This work was partly supported by National Basic Research Program of China (973 Program) (2013CB632403)and Chinese National Science Foundation (21437003).

## Appendix A. Supplementary data

Supplementary data associated with this article can be found, in the online version, at http://dx.doi.org/10.1016/j.apcatb.2016.04.049.

## References

[1] M.A. Shannon, P.W. Bohn, M. Elimelech, J.G. Georgiadis, B.J. Marinas, A.M. Mayes, Nature 452 (2008) 301–310.
[2] M.M. Khin, A.S. Nair, V.J. Babu, R. Murugan, S.A. Ramakrishna, Energy Environ. Sci. 5 (2012) 8075–8109.
[3] G.S. Shao, X.J. Zhang, Z.Y. Yuan, Appl. Catal. B Environ. 82 (2008) 208–218.
[4] M. Ranson, B. Cox, C. Keenan, D. Teitelbaum, Environ. Sci. Technol. 49 (2015) 12951–12957.
[5] J. Xu, Y. Wang, Y. Zhu, Langmuir 29 (2013) 10566–10572.
[6] W. Li, J. Wang, J. Ren, X. Qu, Adv. Mater. 25 (2013) 6737–6743.
[7] Y. Shen, Q. Fang, B. Chen, Environ. Sci. Technol. 49 (2014) 67–84.
[8] R. Daghrir, P. Drogui, D. Robert, Ind. Eng. Chem. Res. 52 (2013) 3581–3599.
[9] Y. Ma, Y. Li, M. Mao, J. Hou, M. Zeng, X. Zhao, J. Mater. Chem. A 3 (2015) 5509–5516.
[10] Z. Huang, F. Li, B. Chen, T. Lu, Y. Yuan, G. Yuan, Appl. Catal. B 136–137 (2013) 269–277.
[11] L.W. Zhang, H.B. Fu, Y.F. Zhu, Adv. Funct. Mater. 18 (2008) 2180–2189.
[12] Y. Zheng, J. Liu, J. Liang, M. Jaroniec, S.Z. Qiao, Energy Environ. Sci. 5 (2012) 6717–6731.
[13] X. Wang, K. Maeda, A. Thomas, K. Takanabe, G. Xin, J.M. Carlsson, K. Domen, M. Antonietti, Nat. Mater. 8 (2009) 76–80.
[14] Y. Wang, X. Wang, M. Antonietti, Y. Zhang, ChemSusChem 3 (2010) 435–439.
[15] Y. Wang, X. Wang, M. Antonietti, Angew. Chem. Int. Ed. 51 (2012) 68–89.
[16] X. Wang, S. Blechert, M. Antonietti, ACS Catal. 2 (2012) 1596–1606.
[17] M. Zhang, J. Xu, R. Zong, Y. Zhu, Appl. Catal. B Environ. 147 (2014) 229–235.
[18] Y. Xu, C.H. Langford, Langmuir 17 (2001) 897–902.
[19] K. Lv, J. Yu, K. Deng, J. Sun, Y. Zhao, D. Du, M. Li, J. Hazard. Mater. 173 (2010) 539–543.
[20] X. Ren, C. Chen, M. Nagatsu, X. Wang, Chem. Eng. J. 170 (2011) 395–410.
[21] Z. Sui, Q. Meng, X. Zhang, R. Ma, B. Cao, J. Mater. Chem. 22 (2012) 8767–8771.
[22] S. Babel, T.A. Kurniawan, J. Hazard. Mater. 97 (2003) 219–243.
[23] H. Gao, Y. Sun, J. Zhou, R. Xu, H. Duan, ACS Appl. Mater. Interfaces 5 (2013) 425–432.
[24] G. Crini, Bioresour. Technol. 97 (2006) 1061–1085.
[25] S. Liu, A. Tang, M. Xie, Y. Zhao, J. Jiang, G. Liang, Angew. Chem. Int. Ed. 54 (2015) 3639–3642.
[26] X. Gao, R.J. Esteves, T.T.H. Luong, R. Jaini, I.U. Arachchige, J. Am. Chem. Soc. 136 (2014) 7993–8002.
[27] D.S. Franklin, S. Guhanathan, J. Appl. Polym. Sci. 132 (2015) 41921–41931.
[28] W. Jiang, Y. Liu, J. Wang, M. Zhang, W. Luo, Y. Zhu, Adv. Mater. Interfaces 3 (2015) 1500502–1500511.

[29] M. Zhang, W. Jiang, D. Liu, J. Wang, Y. Liu, Y. Zhu, Y. Zhu, Appl. Catal. B Environ. 183 (2016) 263–268.
[30] Y. Guo, Y. Wang, C. Hu, Y. Wang, E. Wang, Y. Zhou, S. Feng, Chem. Mater. 12 (2000) 3501–3508.
[31] N. Yan, Z. Zhao, Y. Li, F. Wang, H. Zhong, Q. Chen, Inorg. Chem. 53 (2014) 9073–9079.
[32] Á.A. Beltrán-Osuna, B. Cao, G. Cheng, S.C. Jana, M.P. Espe, B. Lama, Langmuir 28 (2012) 9700–9706.
[33] A. Luchini, D.H. Geho, B. Bishop, D. Tran, C. Xia, R.L. Dufour, C.D. Jones, V. Espina, A. Patanarut, W. Zhou, M.M. Ross, A. Tessitore, E.F. Petricoin, L.A. Liotta, Nano Lett. 8 (2008) 350–361.
[34] Y. Guo, F. Kong, C. Wang, S. Chu, J. Yang, Y. Wang, Z. Zou, J. Mater. Chem. A 1 (2013) 5142–5147.
[35] X. Wang, X. Chen, A. Thomas, X. Fu, M. Antonietti, Adv. Mater. 21 (2009) 1609–1612.
[36] J.X. Sun, Y.P. Yuan, L.G. Qiu, X. Jiang, A.J. Xie, Y.H. Shen, J.F. Zhu, Dalton Trans. 41 (2012) 6756–6763.
[37] M. Alesker, A. Heller, Z. Malik, I. Makarovsky, J.P. Lellouche, J. Mater. Chem. 21 (2011) 10883–10893.
[38] P.V. Zinin, L.C. Ming, S.K. Sharma, V.N. Khabashesku, X. Liu, S. Hong, S. Endo, T. Acosta, Chem. Phys. Lett. 472 (2009) 69–73.